Journal of Power Sources 199 (2012) 418–425

Contents lists available at SciVerse ScienceDirect

Journal of Power Sources

journal homepage: www.elsevier.com/locate/jpowsour

Enhanced efficiency for dye-sensitized solar cells using a surface-treated photo-anode

Rui Liu[a], Wein-Duo Yang[b,*], Liang-Sheng Qiang[a,**]

[a] Department of Applied Chemistry, Harbin Institute of Technology, Harbin 150001, PR China
[b] Department of Chemical and Materials Engineering, National Kaohsiung University of Applied Sciences, Kaohsiung 807, Taiwan

ARTICLE INFO

Article history:
Received 12 June 2011
Received in revised form 19 August 2011
Accepted 18 October 2011
Available online 24 October 2011

Keywords:
TiO_2 nanotube arrays
Anodic oxidation
Surface treatment
Dye-sensitized solar cells

ABSTRACT

Well-ordered TiO_2 nanotube arrays with an inner average pore diameter of 85 nm and a length of 15.69 μm are fabricated by electrochemical anodization in ethylene glycol solution and used as the photo-anode in dye-sensitized solar cells (DSSCs). The photo-conversion efficiency of the DSSCs is significantly enhanced by appropriate surface treatments. The surface of the TiO_2 nanotube arrays is treated with titanium (IV) *n*-butoxide using a hydrothermal method in combination with an oxygen-plasma treatment. The variations in the TiO_2 nanotubes are investigated using field-emission scanning electron microscopy (FESEM), X-ray diffraction (XRD), atomic force microscopy (AFM), contact-angle analysis, X-ray photoelectron spectroscopy (XPS) and electrochemical impedance spectroscopy (EIS). Comparative studies show that the surface area and hydrophilicity are increased, while electron recombination rate is decreased. The TiO_2 nanotube arrays treated by the combined methods under optimum conditions exhibits a conversion efficiency is approximately double that of the untreated TiO_2 nanotube arrays under backside illumination conditions.

1. Introduction

Solar energy finds applications in many fields because of its renewability and recyclability. In 1991, Grätzel and O'Reagan proposed TiO_2-based dye-sensitized solar cells (DSSCs) with low costs and high photo-conversion efficiencies [1]. The TiO_2 nanostructure is an attractive oxide semiconductor material for DSSCs because of its unique electrical and electrochemical properties [2]. DSSCs contain dye molecules, an electrolyte, an anode and a counter electrode. The dye molecules in DSSCs are adsorbed onto the surface of the TiO_2 nanostructures, and the DSSCs are filled with a liquid electrolyte.

The theory of DSSCs can be described as follows: photoexcited dyes inject electrons into the conduction band of TiO_2 due to the higher energy level of dye molecule than conduction band of TiO_2. The loss of electrons from the dye results in the formation of a dye cation (S^+). A small number of electrons are lost by the recombination process, but most are fed into the external circuit through the conductive glass. The oxidized dye (S^+) is reduced by the electrolyte, and the oxidized electrolyte is also reduced by the Pt counter electrode. The entire circuit is powered by the continually regenerated current [3].

The TiO_2 nanoparticles and nanoporous films that form DSSC anodes exhibit 3D randomly packed particle networks. Three-dimensional TiO_2 nanoparticles exhibit good absorbability because of their large specific surface area, but these properties reduce the charge migration and diffusion in photovoltaic devices [4]. A high charge-collection efficiency requires that the transport of photoinjected electrons be faster than the recombination rate [5].

To improve charge transfer and hinder charge recombination, researchers have fabricated one-dimensional TiO_2 nanotube arrays by the electrochemical anodization of Ti foils [6]. Many research groups have concentrated on the DSSCs of TiO_2 nanotube arrays with TiO_2 nanotubes as the anode and a Pt counter electrode as the cathode. DSSCs currently possess two significant disadvantages: a low photoelectric conversion efficiency and a high loss. Considerable effort has been expended on enhancing photo-conversion efficiency; the attempted approaches have included increasing the tube length [7], modifying the TiO_2 nanotube arrays [8], using electrolytes [9] and dyes [10], using front-side illumination [11,12] and treating the TiO_2 nanotubes [13–19].

Liu et al. [7] have fabricated nanotube arrays of different lengths to investigate the effects of the array lengths on the conversion efficiency. Shen et al. [8] have used CdSe-sensitized TiO_2 nanotubes and nanowires to evaluate the optical properties and conversion efficiencies of DSSCs. Flores et al. [9] have used a plasticized polymer electrolyte, which gave an efficiency of 4.03%, at

* Corresponding author. Tel.: +886 73814526x5116; fax: +886 73830674.
** Corresponding author.
E-mail addresses: ywd@cc.kuas.edu.tw (W.-D. Yang), qiangls@sina.com (L.-S. Qiang).

0378-7753/$ – see front matter © 2011 Elsevier B.V. All rights reserved.
doi:10.1016/j.jpowsour.2011.10.072

100 mW cm^{-2}. Shankar et al. [10] have employed donor antenna dyes to improve the efficiency of DSSCs to achieve an efficiency of 6.1% with back-side illumination. In back-side illumination, light intensity is decreased by the counter electrode and the electrolyte, and the transfer of electrons is greatly obstructed by a blocking layer between the TiO_2 and the Ti substrate. For this reason, many researchers choose to use front-side illumination. Mor et al. [11] have sputtered 500 nm titanium films onto FTO (fluorine tin oxide) glass substrates and then grew highly ordered TiO_2 nanotube arrays perpendicular to FTO to generate an efficiency of 2.9%. Chen and Xu [12] have prepared free-standing TiO_2 nanotube arrays that they then transferred onto FTO; the arrays exhibited an efficiency of 5.5% in front-side illumination.

The treatment of TiO_2 nanotube surfaces has become a popular method in recent years. These methods lead to increased surface area, electron transport and dye-loading ability and slow electron recombination. Treatment with $TiCl_4$ has been commonly used to increase the efficiency of DSSCs. Park et al. [13] have used a $TiCl_4$ solution to treat TiO_2 nanotubes; the treatment enhanced charge transfer and improved the conversion efficiency. O'Regan et al. [14] have prepared $TiCl_4$-treated TiO_2 and demonstrated that the efficiency increase is due to the increased quantum efficiency of charge separation at the interface. Roy et al. [15] have used TiO_2 nanoparticles to decorate TiO_2 nanotubes with nanocrystallites with a typical size of 3 nm; significantly higher dye loading was achieved, and the solar cell efficiency was doubled. The treatment of TiO_2 photo-anodes with O_2 plasma has also been reported. Parvez et al. [16] have used O_2 plasma and an ion-beam treatment of nanostructured TiO_2 to enhance the efficiency of DSSCs. Yip et al. [17] have combined the $TiCl_4$ treatment and porous layer deposition for the treatment of tubes; they found that the best performance is obtained when both $TiCl_4$ and the porous layer treatments are used. Kim and Kim [18] have used various overlayers and an O_2-plasma-treated TiO_2 electrode to reduce electron recombination and increase hydrophilicity; the photo-conversion efficiency of the resulting cells was greatly improved. Wang and Lin [19] have employed $TiCl_4$ and O_2 plasma under optimized conditions to treat the surfaces of TiO_2 nanotube arrays and significantly improve the performance of DSSCs.

Surface treatments can improve the efficiency of DSSCs by introducing mixed morphologies and changing some of the properties of the electrodes' surfaces. In this work, we employed titanium (IV) *n*-butoxide (TnB) and oxygen plasma to modify the surfaces and increase the conversion efficiency of DSSCs.

2. Experimental

2.1. Preparation of TiO_2 nanotube arrays

The TiO_2 nanotube arrays were fabricated by the anodization of titanium foils (250 μm thick, 2 cm × 2.5 cm, 99.5% purity) with Pt as the counter electrode. The distance between the two electrodes was 2 cm. The Ti foils were ultrasonically degreased in detergent, acetone, ethanol, deionized water, nitric acid and deionized water for 10 min in sequence. The foils were then dried in an oven prior to anodization. The anodization was performed at room temperature using a Keithley 2400 power source at 40 V for 12 h under magnetic stirring at 150 rpm. The electrolyte contained ethylene glycol, 0.3 wt% ammonium fluoride and 2 vol% water. After anodization, the samples were washed with deionized water and ultrasonically treated to remove precipitates from the surface of the TiO_2 nanotubes. Then the samples were heated to 500 °C in a furnace at atmospheric pressure for 2 h; the heating and cooling rates were both 10 °C min^{-1}.

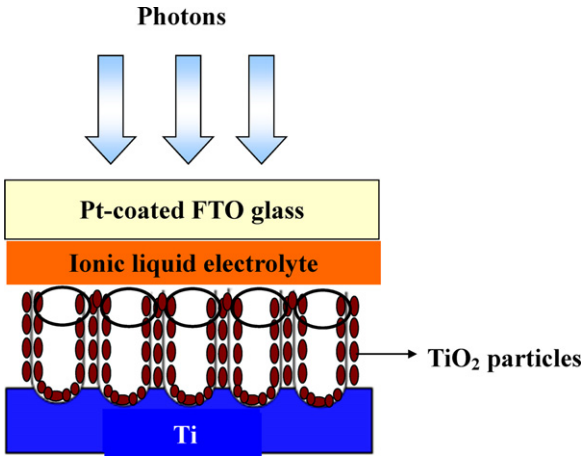

Fig. 1. Schematic illustration of the fabrication of dye-sensitized TiO_2 nanotube solar cells.

2.2. Surface treatment of TiO_2 nanotubes

The calcined TiO_2 nanotubes were treated with TnB using a hydrothermal method. In the hydrothermal process, 15 g of TnB was slowly added to 2 M acetic acid to form a white solution. Hydrolysis and condensation were then performed. After stirring for 4 d, the color of the solution changed from white to transparent. The TiO_2 nanotubes were heated to 200 °C for 5 h, in a Teflon container. After cooling to room temperature, the treated sample was washed with deionized water and heated to 500 °C in a furnace for 30 min at a heating rate of 10 °C min^{-1}. Finally, the nanotubes exposed to O_2 plasma generated with a power of 80 W for different times.

2.3. Fabrication of TiO_2 nanotube solar cells

The TiO_2 nanotubes and treated TiO_2 nanotubes were soaked in 0.5 mM solution of *cis*-diisothiocyanato-bis(2,2′-bipyridyl-4,4′-dicarboxylato)-ruthenium(II)bis(tetra-butylammonium) (N719 dye) at 70 °C for 24 h. The nanotubes were then washed in ethanol to remove nonchemisorbed dye, dried in an oven and calcined at 385 °C for 10 min. A hot-melt polymer (Solaronix SX1170-25, 60 μm) was used as an adhesive spacer. The liquid electrolyte is comprised of 0.1 M LiI, 0.05 M I_2 and 0.5 M 4-*tert*-butylpyridine (TBP) in acetonitrile. The electrolyte was injected between two electrodes and was driven through holes in the hot-melt sealing foil by capillary force. The platinum counter electrode was prepared by spin-coating 5 mM H_2PtCl_6 (in ethanol) onto the FTO glass. The TiO_2 electrode and the counter electrode were appropriately spaced and sealed using hot-melt film as a sandwich spacer. Because Ti foils are not transparent, the light must irradiate the transparent Pt counter electrode. The schematic diagram of configuration of the DSSCs is shown in Fig. 1.

2.4. Characterization

The morphology, length and pore diameter of the TiO_2 nanotubes were investigated with field-emission scanning electron microscope (FESEM, JEOL JSM-7401F) at 5 kV and an amplification ratio of 50,000. The surface roughness was analyzed by atomic force microscopy (BASO-AFM). The crystal structure of the TiO_2 nanotubes was characterized by X-ray diffraction (XRD, PANalytical/X'Pert PRO MPD) using Cu Kα (λ = 0.154 nm) radiation at 10 kV and 100 mA; the samples were scanned from 20° to 80° 2θ. The contact angle is defined as the angle between the solid surface and a tangent to the drop-surface. The advancing

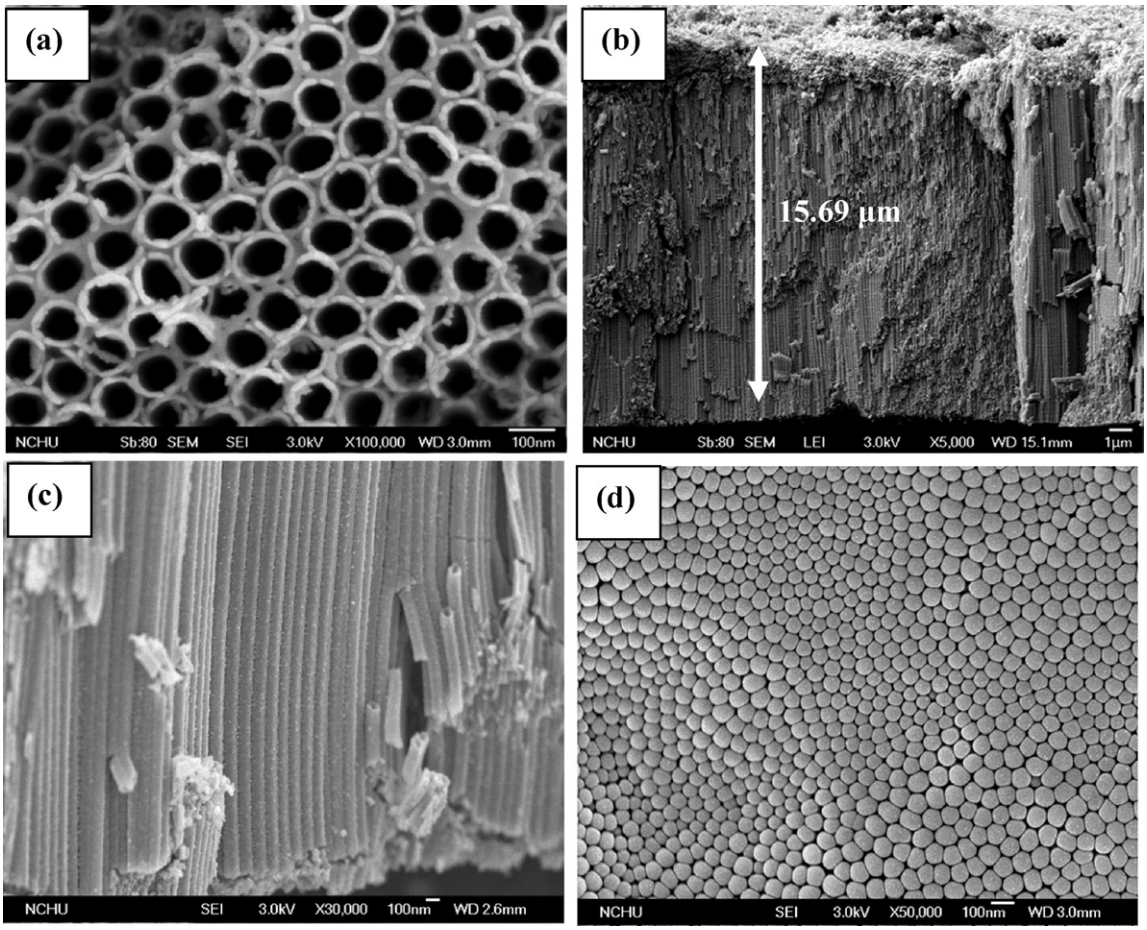

Fig. 2. FESEM images of TiO_2 nanotube arrays: (a) top, (b) cross-sectional, (c) magnified cross-sectional and (d) bottom views.

contact angles of expanding droplets were determined using a Digidrop contact-angle measuring device. The O_2 plasma generator (Dressler, Cesar-136) was operated under a vacuum of 500 mtorr at 80 W. The amounts of dye loading were determined using UV–vis spectroscopy (Jasco V-600); the samples were placed into 10 mM KOH to desorb the dye. The slit width was 2.0 mm, the step was 0.5 nm, and the scanned wavelength range was 250–800 nm. X-ray photoelectron spectroscopy (XPS, Kratos Axis Ultra DLD) patterns were obtained using a monochromatic Al-anode X-ray gun. Photocurrent–voltage characteristics were measured under simulated solar light (AM 1.5, 100 mW cm^{-2}) using a Keithley 2400 sourcemeter; the active area of the solar cells was 0.25 cm^2. Electrochemical impedance spectra (EIS) are measured at open circuit voltage with a bias of 10 mV in frequency from 10^{-1} to 10^5 Hz to analyze the electron transport properties. An appropriate equivalent circuit model is employed to fit the impedance spectra of TiO_2 naotubes photo-anode by ZsimpWin software.

3. Results and discussion

Fig. 2 shows typical FESEM images for the TiO_2 nanotube arrays. The average inner diameter of the TiO_2 nanotube arrays is 85 nm, the average wall thickness is 10 nm (Fig. 2a), and the average tube length is 15.69 μm (Fig. 2b). As evident in the figures, the pores are uniform and closely packed. The magnified cross-sectional image (Fig. 1c) shows straight and smooth tube walls, and the bottom view (Fig. 1d) indicates that the bottoms of tubes are closed well. However, the FESEM images of the TiO_2 nanotubes treated by TnB using the hydrothermal method indicate the formation of some additional materials on the top surface, as shown in Fig. 3a. The additional materials may be TiO_2 nanoparticles, and Fig. 3c also shows that some TiO_2 particles were grown on the tube wall. These TiO_2 particles can increase the surface area to allow higher dye adsorption. However, they can also form a very thin blocking film, in which case the scattering of free electrons and the trapping of electrons at the interfaces may enhance charge transport and reduce charge recombination. The diagram [20] in Fig. 4 demonstrates the effect of the TnB treatment. As the schematic illustrates the thin film can theoretically be formed during the cycling process. In practice, the amounts of TiO_2 nanoparticles need to be optimized because the blocking film is too thick to transport electrons, i.e., it may increase charge recombination. The tube length of TnB-treated TiO_2 nanotubes is not significantly changed. The morphology of combined O_2 plasma-treated TiO_2 nanotubes also do not change (figure is not given).

On the basis of the SEM images, we have estimated the approximate surface roughness factor (rf) of the TiO_2 nanotubes. Eq. (1) is shown as follows [3]:

$$\mathrm{rf} = \frac{4\pi(dp + \omega)}{\sqrt{3}l^2} \quad (1)$$

where dp, l and ω are the pore inner diameter, the distance between centers of TiO_2 nanotube arrays and wall thickness, respectively. Because of the closely packed and compact structure of the TiO_2 nanotubes, they can be assumed to be idealized structures, i.e., the spacing between the tubes is assumed to be zero. Based on Eq. (1), the estimated roughness factor of the TiO_2 nanotubes is 62.48. In case of TnB-treated TiO_2 nanotubes, the pores are irregular, which precludes the use of Eq. (1) to estimate the roughness factor.

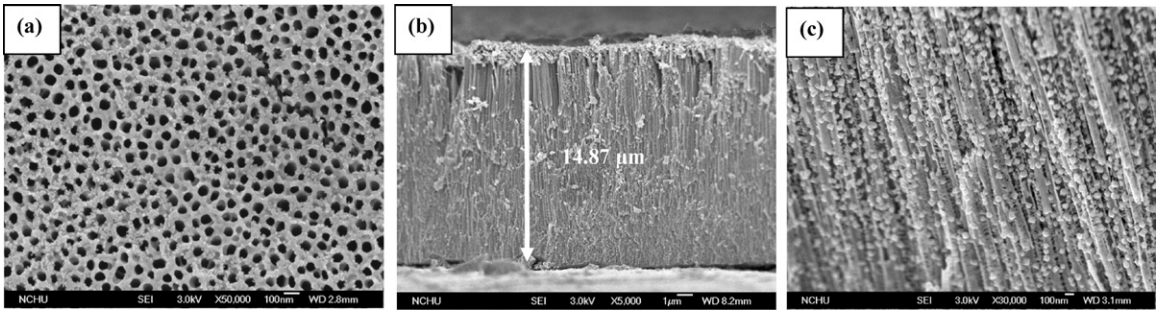

Fig. 3. FESEM images of TnB-treated TiO_2 nanotube arrays: (a) top, (b) cross-sectional and (c) magnified cross-sectional views.

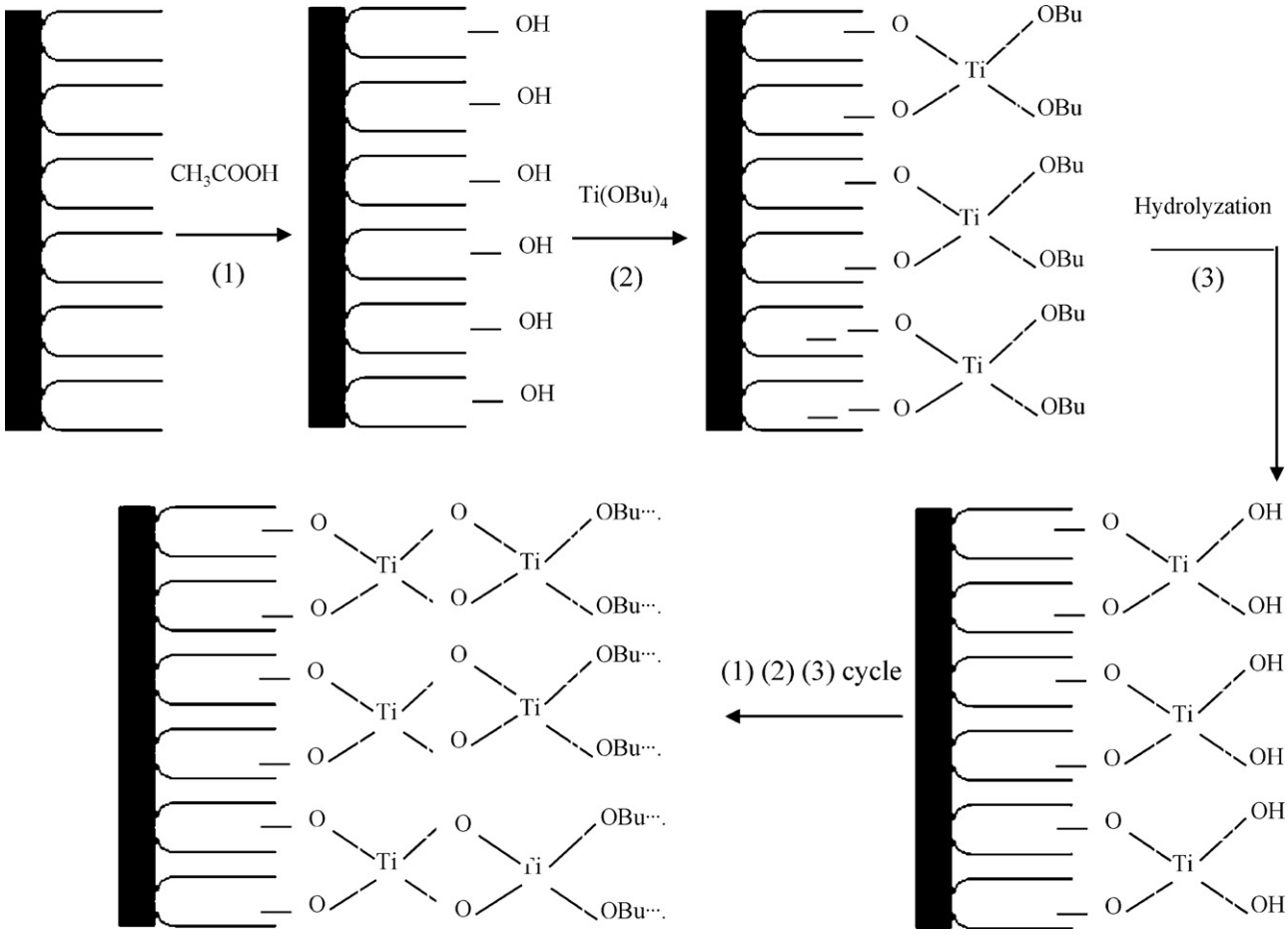

Fig. 4. Schematic diagram of the formation of TiO_2 thin films on the TiO_2 nanotube arrays.

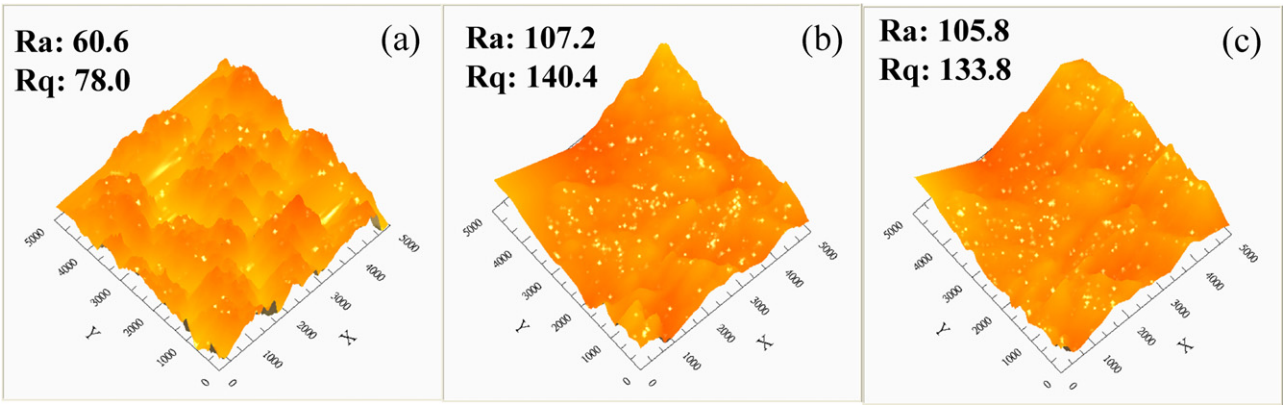

Fig. 5. AFM analysis of (a) TiO_2 nanotubes, (b) TnB-treated TiO_2 nanotubes and (c) TnB and O_2 plasma-treated TiO_2 nanotubes.

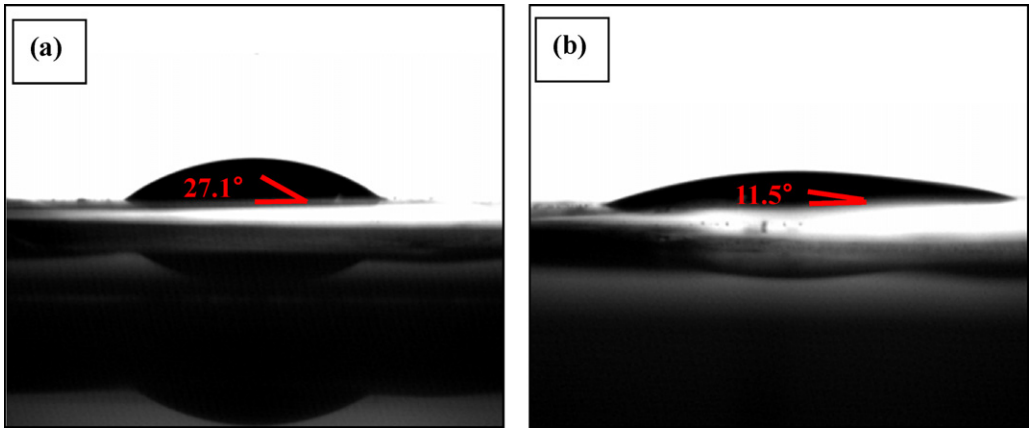

Fig. 6. The contact angle analyzed pattern of (a) TiO_2 nanotubes and (b) TnB and O_2 plasma-treated TiO_2 nanotubes.

The surface topography and roughness were further investigated by atomic force microscopy (AFM). The 3-D AFM images of TiO_2 nanotubes and TnB-treated TiO_2 nanotubes are shown in Fig. 5. The root mean square parameter (Rq) and the average roughness (Ra) are 140.4 and 107.2 for the TnB-treated TiO_2 nanotubes and 78 and 60.6, respectively, for the TiO_2 nanotubes. The average roughness of the TiO_2 nanotubes is consistent with the calculated value. As evident in Fig. 5, the difference in the roughness factors between the TnB-treated TiO_2 nanotubes and the TiO_2 nanotubes arises from the surface treatment. However, slightly less roughness was observed after the 10 min O_2 plasma treatment was applied, which indicates that the O_2 plasma treatment reduced the surface contamination. The higher roughness factor indicates that the treated TiO_2 nanotubes exhibited a higher specific surface area. The larger the roughness factor is, the greater the adsorption of the dye.

Fig. 6 shows the contact angle measurements for the TiO_2 nanotubes and the combination-treated TiO_2 nanotubes. The contact angle decreased from 27.1° to 11.5°, which indicates that the hydrophilicity was increased after the 10 min O_2 plasma treatment. Tsoi et al. [21] have demonstrated that O_2 plasma treatment is an effective technique for saturating the metal-oxide surface with hydroxyl groups. According to the rule of similarity, there is a strong interaction between hydroxyl groups and water molecules,

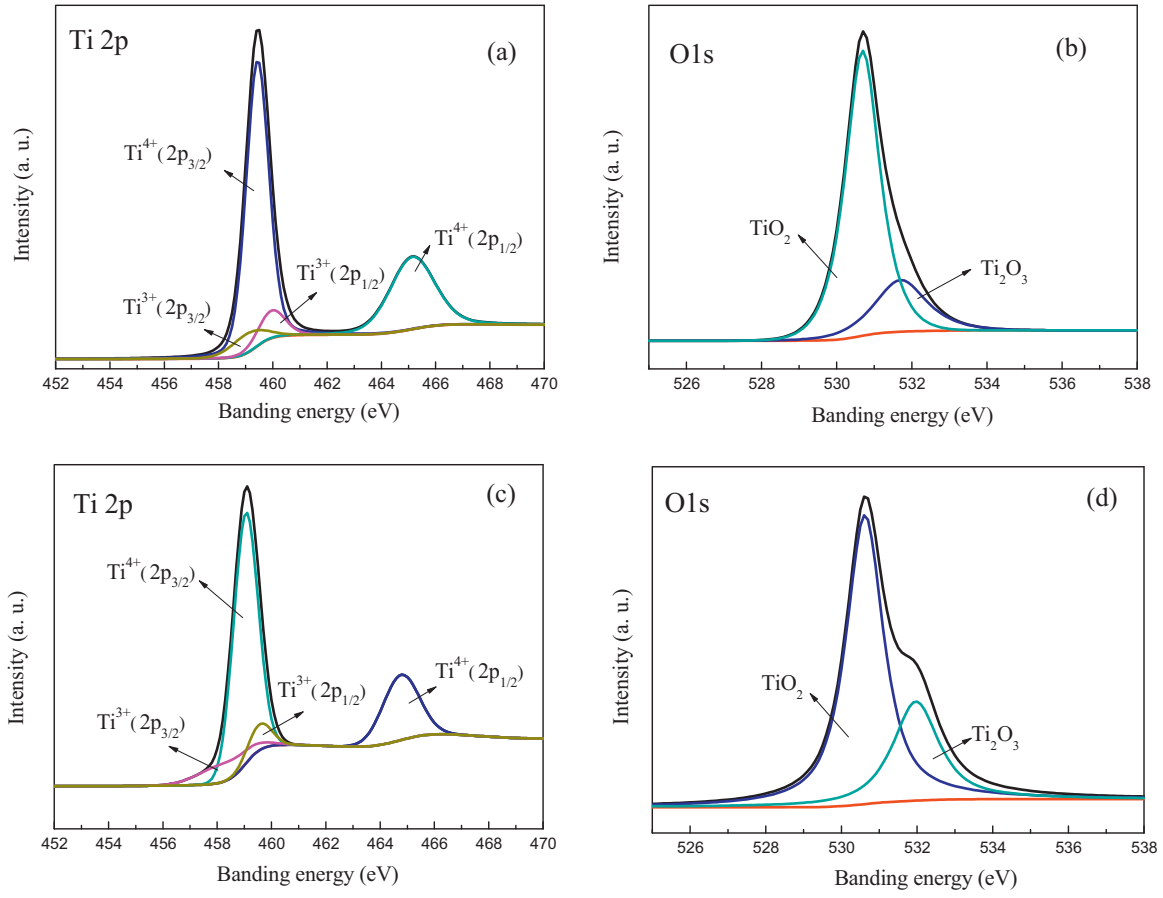

Fig. 7. High-resolution XPS spectra of (a and b) TiO_2 nanotubes and (c and d) TnB and O_2 plasma-treated TiO_2 nanotubes.

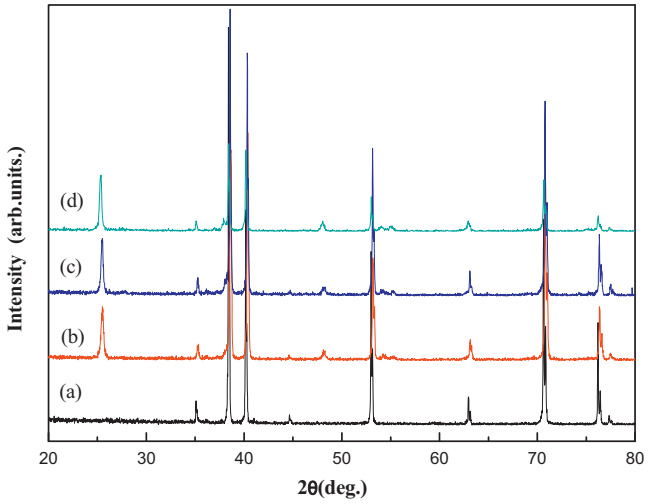

Fig. 8. XRD patterns of samples: (a) uncalcined, (b) TiO_2 nanotubes calcined at 500 °C, (c) TnB-treated TiO_2 nanotubes and (d) TnB- and O_2 plasma-treated TiO_2 nanotubes.

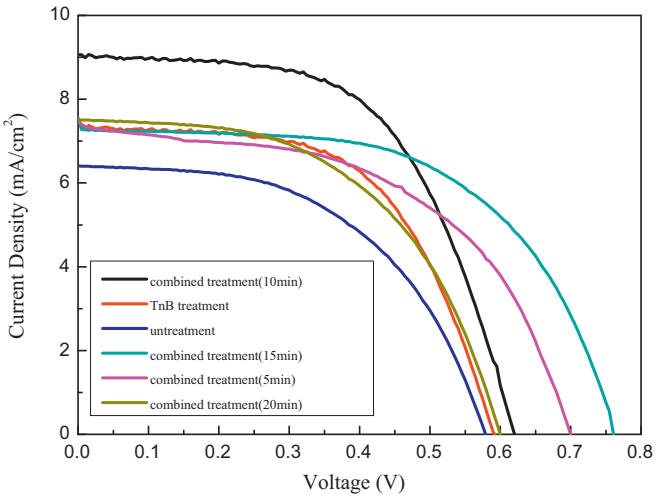

Fig. 9. Current–voltage characteristics of dye-sensitized TiO_2 nanotube solar cells.

which increases hydrophilicity and facilitates the adsorption of dye. Park and Dhayal [22] have reported that O_2 plasma treatment can increase hydrophilicity because of the increased number of carboxylic groups at the surface of TiO_2.

XPS was used to examine the change of the surface charge states of TiO_2 nanotubes and functionalities at the surface. High-resolution Ti (2p) and O (1s) XPS spectra of TiO_2 nanotubes and O_2 plasma-treated nanotubes are shown in Fig. 7. The Ti (2p) XPS spectra of the TiO_2 nanotubes and the TiO_2 nanotubes treated with 10 min O_2 plasma exhibited four peaks. The surface stoichiometry was determined by calculating the relative peaks of the total areas for Ti (2p) and O (1s). Table 1 summarizes the stoichiometric values of the atomic contents of the different valence states. Approximately 87.6% of the titanium surface state for the Ti (2p) peaks for the untreated TiO_2 nanotubes was Ti^{4+}. The Ti^{3+} surface state for Ti (2p) was increased from 12.4% to 15.3% after the combined treatments, in which the reaction TiO_2 (Ti^{4+}) → Ti_2O_3 (Ti^{3+}) occurs at the surface of the TiO_2 nanotubes. The relative change is also observed in the O (1s) XPS spectra. The ratio of the Ti_2O_3 peak areas increased from 21% to 29.5% after the combined treatments. This result suggests that the higher oxidation states (Ti^{4+}) were reduced to Ti^{3+}. The reduction of Ti^{4+} to Ti^{3+} also generated oxygen vacancies and redundant electrons, which can change the electronic structure. The O_2 plasma treatment can generate various species, such as O^-, O_2^-, O^+ and O_2^+ ions, $H^\bullet$ and $OH^\bullet$ radicals and energetic photons. The O^+ and O_2^+ species oxidize Ti^{3+} ions to Ti^{4+} in TiO_2 nanotubes. The introduction of O^- and O_2^- species reduced Ti^{4+} to Ti^{3+} states, which supported the transport of electrons and holes between dye molecules and the photo-anode after the combined treatments. Carboxyl functionality was simultaneously increased, which indicates that the interaction between the carboxylic groups and the dye molecules was strengthened, in accordance with the results of Park and Dhayal [22].

XRD was used to confirm the crystal phases of the TiO_2 nanotubes and the treated TiO_2 nanotubes that were annealed at 500 °C for 2 h. The results are shown in Fig. 8. In the absence of annealing, the as-anodized TiO_2 nanotubes are amorphous, and only the diffraction peaks of the Ti substrate are evident, as reported in previous studies [23]. For the nanotubes annealed at 500 °C, the characteristic peaks at 25.28° and 48.04° can be assigned to the (2 0 0) and (1 0 1) planes, respectively, of the anatase phase. For the samples treated with TnB and 10 min O_2 plasma, the peaks are similar to the untreated sample, which indicates that surface modification has no influence on the crystallization of the TiO_2 nanotubes. This result also confirms that the as-formed TiO_2 particles are converted to the anatase phase after the particles have been annealed at 500 °C for 2 h.

To verify the amounts of dye absorption, UV–vis spectroscopy measurements were performed on the desorbed dyes. On the basis of Beer's law, the dye loading can be obtained by fitting the absorption at 510 nm to the calibration curve. The dye loading values are listed in Table 2. For only TnB treatment, dye loading is increased to 4.98×10^{-8} mol cm^{-2}. This probably arises from the fact that formed TiO_2 particles can increase the surface area to allow higher dye absorption. Combined surface treatments result in higher dye absorption, and the best results were obtained with both TnB and 10 min oxygen plasma treatments. The properly combination-treated TiO_2 nanotubes exhibit a greater hydrophilicity and a greater surface area, which results in a greater absorption of dye molecules. However, amounts of dye absorption were decreased with increasing to 15 min O_2 plasma exposures, which are likely attributed to the lower surface roughness and hydrophilic ability after longer time O_2 plasma treatment. Another possible reason is that the number of oxygen vacancies increases for prolonged plasma exposure by XPS analysis, leading to decreased electrostatic interaction between the Ti^{4+} sites in TiO_2 and carboxylic groups of the N719 dye. The weaker interaction of between the TiO_2 nanotubes and dye can reduce the dye loading.

In general, good DSSCs exhibit three features: higher dye adsorption, a lower recombination of electrons and immediate electron transport. Fig. 9 shows the effects of TnB and different O_2 plasma treatment times on the *I–V* characteristics of DSSCs. The electron lifetime (τ) was determined by electrochemical impedance spectroscopy (EIS). To see clearly, bode plots of the

Table 1
XPS relative peak areas with respect to the total area of the Ti 2p and O 1s peaks for untreated and combination-treated TiO_2 nanotubes.

Sample	Ti^{4+} ($2p_{1/2}$)	Ti^{4+} ($2p_{3/2}$)	Ti^{3+} ($2p_{1/2}$)	Ti^{3+} ($2p_{3/2}$)	TiO_2	Ti_2O_3
Untreated (%)	29.1	58.5	6.7	5.7	79.0	21.0
Treated (%)	23.5	61.2	9.3	6.0	70.5	29.5

Table 2
Photovoltaic performance of DSSCs under AM-1.5 illumination.

Surface treatment	Dye loading (mol cm^{-2})	τ (ms)	V_{oc} (V)	J_{sc} (mA cm^{-2})	Fill factor	η (%)
No	3.53×10^{-8}	8.8	0.575	6.40	0.513	1.89
TnB	4.98×10^{-8}	32.4	0.590	7.34	0.561	2.43
TnB and O_2 plasma (5 min)	5.54×10^{-8}	76.2	0.700	7.45	0.605	3.15
TnB and O_2 plasma (10 min)	7.48×10^{-8}	46.8	0.620	9.06	0.577	3.24
TnB and O_2 plasma (15 min)	6.01×10^{-8}	133.8	0.761	7.56	0.641	3.68
TnB and O_2 plasma (20 min)	5.97×10^{-8}	40.9	0.600	7.50	0.620	2.79

obtained data are exhibited in Fig. 10(A) and (B), respectively. Generally, there are three frequency peaks – low (in the range of mHz), medium (in the range at 1–100 Hz) and high (in the range of kHz) frequency peak. The high frequency peak is attributed to the charge transfer at the counter electrode, and the low frequency peak is associated with the diffusion in the electrolyte. The electron transport in TiO_2 nanotubes and charge reaction at the TiO_2/electrolyte interface are reflected in the medium frequency. The corresponding characteristic mid-frequency peak (f_{max}) for TiO_2 nanotubes, TnB, TnB and 5 min O_2 plasma, 10 min O_2 plasma, 15 min O_2 plasma and 20 min O_2 plasma treatment located at 18 Hz, 4.9 Hz, 2.09 Hz, 3.4 Hz, 1.19 Hz and 3.89 Hz, respectively. The electron lifetime can be estimated by the medium frequency as Eq. (2) [24,25]: The corresponding values are also summarized in Table 2. For the untreated TiO_2 nanotubes, DSSCs exhibited a J_{sc} value of 6.40 mA cm^{-2}, a V_{oc} value of 0.575 V and a fill factor (FF) of 0.513, to give an overall conversion efficiency of 1.89%. When TnB was incorporated into the surface and tube wall of the TiO_2 nanotube arrays, the conversion efficiency of the DSSCs was 2.43%, with a J_{sc} of 7.34 mA cm^{-2}, a V_{oc} of 0.590 V and a FF of 0.561. As can be seen, the J_{sc} value was increased as it indicates that the presence of TiO_2 nanoparticles allows high dye absorption by TnB treatment. The more electrons were injected from the dye to the conduction band of the TiO_2 nanotubes with increasing dye absorption, which resulted in the higher light harvesting. The V_{oc} value is slightly enhanced. That is because that a thin blocking layer of TiO_2 nanoparticles formed on the TiO_2 nanotubes and an uncovered region of Ti substrate increase immediate electron transport from the tube walls to the bottom of TiO_2 nanotubes. The blocking layer and uncovered substrate also decrease the surface charge recombination. Moreover, it can diffuse more redox species inside the pores after TnB treatment, which leads to an increased electron lifetime. As a result, the conversion efficiency is enhanced. After the combined TnB and 5 min O_2 plasma treatments, the overall conversion efficiency of the DSSCs was increased to 3.15%, with a J_{sc} of 7.45 mA cm^{-2}, a V_{oc} of 0.700 V and a FF of 0.605.

$$\tau = \frac{1}{2\pi f_{max}} \tag{2}$$

An effective enhancement of V_{oc} was achieved by the O_2 plasma treatment. The open-circuit voltage (V_{oc}) depends on the electron lifetime, as shown in Eq. (3):

$$\tau = \frac{-k_B T}{e}\left[\frac{dV_{oc}}{dt}\right]^{-1} \tag{3}$$

where $k_B T$ is the thermal energy, e is the positive elementary charge, and dV_{oc}/dt is the derivative of the V_{oc} transient, in which the V_{oc} value is corresponding to electron lifetime. The electron lifetime for TnB and 5 min O_2 plasma treatment is much longer than TnB treatment. It can be explained that the O_2 plasma treatment maybe occur discharge reaction at the surface: $TiO_2 + h\nu \rightarrow TiO_2^*(h_{vb}^+ e_{cb}^-)$, where the number of electrons in conduction band of TiO_2 nanotubes is increased [22]. Excess electrons can increase potential between Fermi energy of TiO_2 nanotubes and redox couple of electrolyte, that is reduced the recombination rate. Combined surface treatment on TiO_2 photo-anodes not only increased the dye loading but also increased electron lifetime between injected electrons in the TiO_2 conduction band and I_3^- in the electrolyte.

The most interesting finding is exceptional performance of DSSCs for 10 min O_2 plasma treatment. Although the conversion efficiency and J_{sc} value was increasing as elongating the O_2 treatment time up to 10 min, the V_{oc} value was decreased sharply. The great improvement of J_{sc} value should be attributed to the highest dye absorption and an increased light harvesting. However, the increase adsorbed dye molecules would produce more

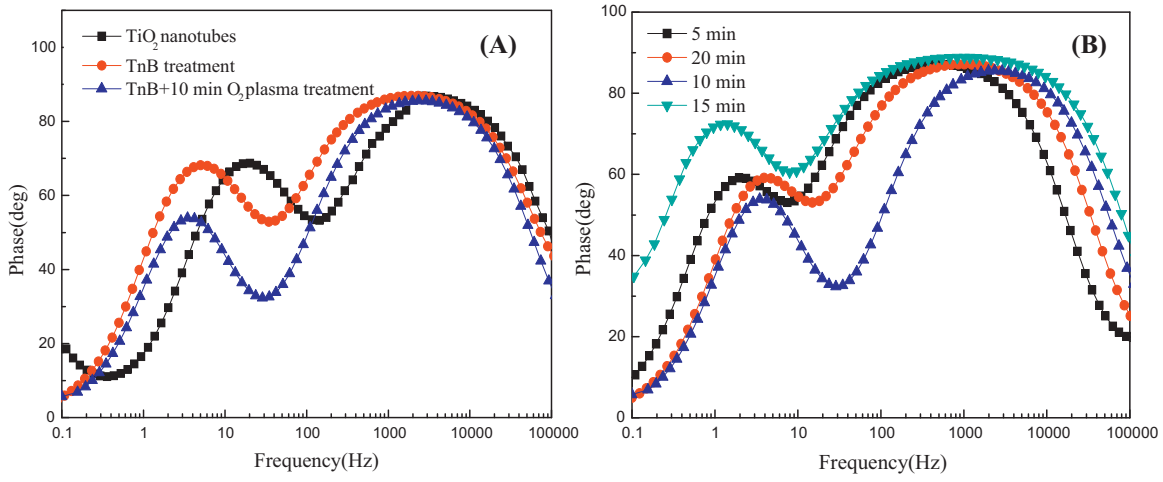

Fig. 10. Electrochemical impedance spectroscopy (EIS) results (Bode plots) of TiO_2 nantoubes and treated TiO_2 nanotubes.

recombination sites, resulting in a lowed V_{oc} and electron lifetime. The two effects appeared to be competitive each other, in which extent of the increase in J_{sc} is much greater than the extent of the decrease in V_{oc}. Therefore, the overall conversion efficiency shows a systematic increase with increasing the time of O_2 plasma exposure.

The highest efficiency was 3.68%, almost double the conversion efficiency of TiO_2 nanotube arrays, for a 15 min O_2 plasma exposure, with a J_{sc} of 7.56 mA cm^{-2}, a V_{oc} of 0.761 V and a FF of 0.641. Although J_{sc} is a little lower, V_{oc} achieves the peak value. However, the conversion efficiency could not further enhance with increasing to 20 min O_2 plasma treatment. The O_2 plasma treatment can generate various species, such as O^-, O_2^-, O^+ and O_2^+ ions, and the amounts of each species can vary with the exposure time of O_2 plasma. This result may be due to the formation of more O^- and O_2^- species during prolonged plasma exposures, leading to an increased the number of oxygen vacancies. Oxygen vacancies are beneficial to a recombination of electrons between the conduction bands of TiO_2 nanotubes and the I_3^- ions of the electrolyte [26]. The electron lifetime and V_{oc} value consequently decreased. The conversion efficiency might be further increased with a longer tube structure, a different electrolyte composition and front-side illumination.

4. Conclusion

We have employed an optimal surface-treatment technique to improve the efficiency of DSSCs. The surfaces of the TiO_2 nanotubes were treated with TnB using a hydrothermal method in combination with an oxygen plasma treatment. SEM and AFM analysis confirmed the presence of a barrier layer formed by TiO_2 nanoparticles on the TiO_2 nanotubes. The O_2 plasma treatments increased the surface hydrophilicity and the amount of Ti^{3+} sites, as determined by contact-angle and XPS measurements. On the basis of UV–vis absorption spectra, dye absorption was increased by the combined TnB and O_2 plasma treatments. The effect of the combined treatments also enhanced the V_{oc} and J_{sc} values, which resulted in an approximate doubling of the conversion efficiency relative to the untreated TiO_2 nanotube arrays. This technique offers a feasible method to improve the efficiency of DSSCs and provides a starting point for further applications.

Acknowledgement

The authors would like to express their gratitude to the National Science Council of Taiwan for supporting this research under Grant No. 96-2221-E-151-050-MY3.

References

[1] B. O'Regan, M. Grätzel, Nature 353 (1991) 737–740.
[2] M. Grätzel, Nature 414 (2001) 338–344.
[3] K. Zhu, N.R. Neale, A. Miedaner, A.J. Frank, Nano Lett. 7 (2007) 69–74.
[4] K.D. Benkstein, N. Kopidakis, J.V.D. Lagemaat, A.J. Frank, J. Phys. Chem. B 107 (2003) 7759–7767.
[5] P. Charoensirithavorn, Y. Ogomi, T. Sagawa, S. Hayase, S. Yoshikawa, J. Cryst. Growth 311 (2009) 757–759.
[6] M. paulose, G.K. Mor, O.K. Varghese, K. Shankar, C.A. Grimes, J. Photochem. Photobiol. A 178 (2006) 8–15.
[7] Z.Y. Liu, V. Subramania, M. Misra, J. Phys. Chem. C 113 (2009) 14033–14208.
[8] Q. Shen, T. Sato, M. Hashimoto, C.C. Chen, T. Toyoda, Thin Solid Films 499 (2006) 299–305.
[9] I.C. Flores, J.N. Freitas, C. Longo, A.F. Nogueira, J. Photochem. Photobiol. A 189 (2007) 153–160.
[10] K. Shankar, J. Bandara, M. Paulose, H. Wietasch, O.K. Varghese, G.K. Mor, C.A. Grimes, Nano Lett. 8 (2008) 1654–1659.
[11] G.K. Mor, K. Shankar, M. Paulose, O.K. Varghese, C.A. Grimes, Nano Lett. 6 (2006) 215–218.
[12] Q.W. Chen, D.S. Xu, J. Phys. Chem. C 113 (2009) 6310–6314.
[13] H. Park, W.R. Kim, H.T. Jeong, J.J. Lee, H.G. Kim, W.Y. Choi, Solar Energy Mater. Solar Cells 95 (2011) 184–189.
[14] B.C. O'Regan, J.R. Durrant, P.M. Sommeling, N.J. Bakker, J. Phys. Chem. C 111 (2007) 14001–14010.
[15] P. Roy, D. Kim, I. Paramasivam, P. Schmuki, Electrochem. Commun. 11 (2009) 1001–1004.
[16] M.K. Parvez, G.M. Yoo, J.H. Kim, K.J. Ko, S.R. Kim, Chem. Phys. Lett. 495 (2010) 69–72.
[17] C.T. Yip, C.S.K. Mak, A.B. Djurisic, Y.F. Hsu, W.K. Chan, Appl. Phys. A 92 (2008) 589–593.
[18] J.T. Kim, S.H. Kim, Solar Energy Mater. Solar Cells 95 (2011) 336–339.
[19] J. Wang, Z.Q. Lin, Chem. Mater. 22 (2010) 579–584.
[20] Y.T. Liu, R.H. Liu, C.B. Liu, S.L. Luo, L.X. Yang, J. Hazard. Mater. 182 (2010) 912–918.
[21] S. Tsoi, E. Fok, J.C. Sit, J.G.C. Veinot, Langmuir 20 (2004) 10771–10774.
[22] K.H. Park, M. Dhayal, Electrochem. Commun. 11 (2009) 75–79.
[23] Y.F. Jia, H.H. Zhou, P. Luo, S.L. Luo, J.H. Chen, Y.F. Kuang, Surf. Coat. Technol. 201 (2006) 513–518.
[24] R. Kern, R. Sastrawan, J. Ferber, R. Stangl, J. Luther, Electrochim. Acta 47 (2002) 4213–4225.
[25] Q. Wang, J.E. Moser, M. Grätzel, J. Phys. Chem. B 109 (2005) 14945–14953.
[26] Y. Kim, B.J. Yoo, R. Vittal, Y. Lee, N.G. Park, K.J. Kim, J. Power Sources 175 (2008) 914–919.